THE PUBLISHING HOUSE
OF THE ROMANIAN ACADEMY

PROCEEDINGS OF THE ROMANIAN ACADEMY, Series A,
Volume 11, Number 2/2010, pp. 125–136

THE TURBULENT BOUNDARY LAYER ON WIND TURBINE BLADES

Horia DUMITRESCU, Vladimir CARDOŞ

"Gh. Mihoc-C. Iacob" Institute of Statistical Mathematics and Applied Mathematics
Corresponding author: Horia DUMITRESCU, E-mail: horiad12@yahoo.com

The short separation bubbles which form near the leading edge of the inboard sections of the blade prior to the onset of leading edge stall have been analyzed in detail, including some effects of viscous-inviscid interaction. The separated laminar shear layer and turbulent reattaching flow are represented by an integral formulation. The transition point is assumed to correspond to the minimum skin friction. Solutions are obtained using an interactive procedure for four cases of large adverse gradient flows. Results obtained for the leading edge separation bubbles showed that the rotational augmentation of blade lift was linked to specific separation and reattachment behaviors, and to pumping effect in the rotational central flow like a rotating disk in axial flow.

Key words: Three-dimensional turbulent boundary layer; Boundary layer separation; Rotational effects.

1. INTRODUCTION

The regions of separated flow which form on blades govern the blade stall characteristics and the loading of wind turbine blades. The nature and extent of these regions are determined primarily, except for the airfoil shape, incidence and Reynolds number, by the two most important parameters that trigger three-dimensional effects and are the radius by chord ratio *r/c* and the rotation parameter V_w / Ω_r which represents the ratio of the wind velocity to the tangential velocity. The rotation parameter shows the interaction between the axial flow (wind) and the rotational flow induced by the rotor blades, and can also be interpreted as ratio between centrifugal forces and Coriolis forces. The physical mechanism driving all the three-dimensional effects is in conjunction with the interaction between the wind speed higher than the design velocity and the flow induced by constant-rotational speed rotors. If the rotation parameter is less one along the entire span ($V_w / \Omega_r < 1$) and for properly twisted blades the flow is generally attached and non-affected by it. Stronger Coriolis force means less adverse pressure gradients that accelerate the flow in the chordwise direction towards the trailing edge. But the wind turbine blades often operate in deep stall with $V_w / \Omega_r > 1$ at the inner part of the span producing both strong centrifugal and Coriolis forces that involve the separation of the boundary layer on blade. Stronger centrifugal force means the increase in the total pressure in flow that reduces the negative pressure peak from the leading edge and produces leading-edge separation bubbles (non leading edge stall). The Coriolis forces, also augmented, induce a spanwise spinning flow in the separated area and contribute to stall-delay by a favorable chordwise pressure gradient. The occurrence of what is turned inboard stall-delay, characterized by an abrupt increase in lift and drag, can be attributed to the sudden suck of air from the separation bubble at the leading edge of blade and driven it towards the radial direction. Of concern here are the small separation bubbles which form near the leading edge of the inboard sections of the blade, at *r/c* = 1. At extreme inboard locations, separation bubble initiation and aft progression are closely associated with post stall lift force magnitudes that exceed those exhibited by nonrotating blades.

The flow in the vicinity of the leading edge of a blade section subject to leading-edge stall is as sketched in Fig. 1. The laminar boundary layer, extending from the stagnation point over the leading edge, separates just downstream of the point of minimum pressure. Transition to turbulent flow occurs in the free

shear layer a short distance downstream of the separation point. The flow then reattaches to the section surface, with a turbulent boundary layer extending from the reattachment point to the trailing edge. If the *r/c* ratio is decreased, the bubble becomes slightly shorter and ultimately coalesces in a singular point [1, 2]. The specific mechanism for bubble absorption is not presently known. It has been assumed though, that there is such a variation in the Coriolis force and the spanwise pressure gradients so that the bubble is suppressed when a limit is exceeded and the flow is completely stabilized against separation [3].

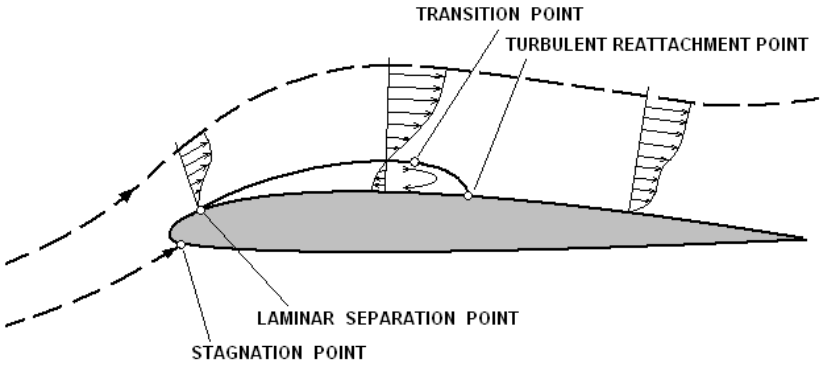

Fig. 1 – Flow in the vicinity of leading edge bubble.

Numerical investigation of three-dimensional and rotational effects on wind turbine blades is today limited to larger radial distances $r/c > 1$, because at the root area of the blade ($r = 1$) some terms are neglected or can not be accurately valued [4, 5, 6]. It should be noted that the effects of the all secondary terms are important in understanding the underlying physical mechanism which triggers the 3-D and the rotational effects. In this study, the separated and reattaching shear layer in a leading-edge bubble on wind turbine blade is analyzed using a full integral formulation assuming that the boundary-layer approximation is applicable. Interaction between the viscous and inviscid flows in the vicinity of bubble is taken into account through a simplified procedure.

2. REPRESENTATION OF FLOW ELEMENTS

A three-dimensional model has been devised in order to identify the influence of the three-dimensional and rotational effects on the blade section characteristics. The incompressible three-dimensional boundary layer equations are written in integral form in the cylindrical coordinate system, (θ, r, z) which rotates with the blade with a constant rotational speed Ω (Fig. 2). θ denotes the peripheral, r the radial (blade spanwise) and z the axial direction.

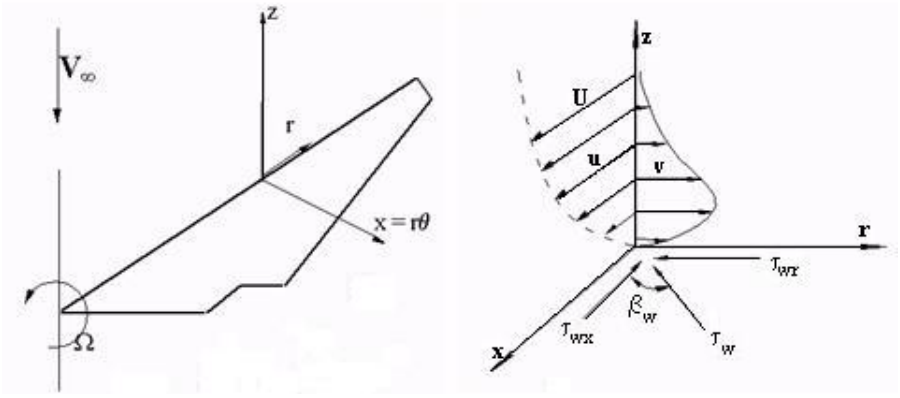

Fig. 2 – Cylindrical coordinate system and notation used.

2.1. Inviscid flow

In order to find the velocity at the airfoil surface in absence of viscous effects, the reference velocity at a point on a rotating wind turbine blade is

$$U_r = \sqrt{V_w^2 + (\Omega r)^2}\ , \tag{1}$$

where V_w is the wind velocity.

From the idea of Fogarty and Sears [7], an inviscid edge velocity can be calculated as

$$U = \Omega_z r \frac{\partial \phi}{\partial \theta},\ V = \Omega_z (\phi - 2\theta),\ W = \Omega_z r \frac{\partial \phi}{\partial z}, \tag{2}$$

where $\phi = \phi(\theta, z)$ denotes the 2-D potential solution, that is constant at all radial positions The interesting point regarding to the equation (2) is that the spanwise component V can be derived from the local two-dimensional velocity potential. However, this spanwise component is very small and thus neglected in the present study. The potential edge velocity components can be approached as

$$U_e = U_r U_a, V = 0\ , \tag{3}$$

where the velocity U_a could be obtained by a viscous-inviscid interaction procedure for flow past a two-dimensional airfoil [8].

However, the primary objective of the present study is to investigate the leading-edge separation bubble on stalled blade by means of the boundary layer method. To achieve this objective the velocity U_a is simply considered a linear adverse velocity gradient near the leading edge which behind the separation relaxes with the vanishing skin-friction. Therefore, the following flow is applied to solve

$$U_e = U_r \left(1 - k\frac{x}{c}\right),\ \text{for}\ \frac{x}{c} \le \left(\frac{x}{c}\right)_{sep}\ , \tag{4}$$

$$U_e \delta_{2x}^{1/(H+2)} = \text{const.},\ \text{for}\ \frac{x}{c} \ge \left(\frac{x}{c}\right)_{sep}\ , \tag{5}$$

where c is the chord length, k is a velocity gradient like parameter, and δ_{2x}, H are the momentum thickness and the boundary-layer shape parameter in the streamwise direction, respectively.

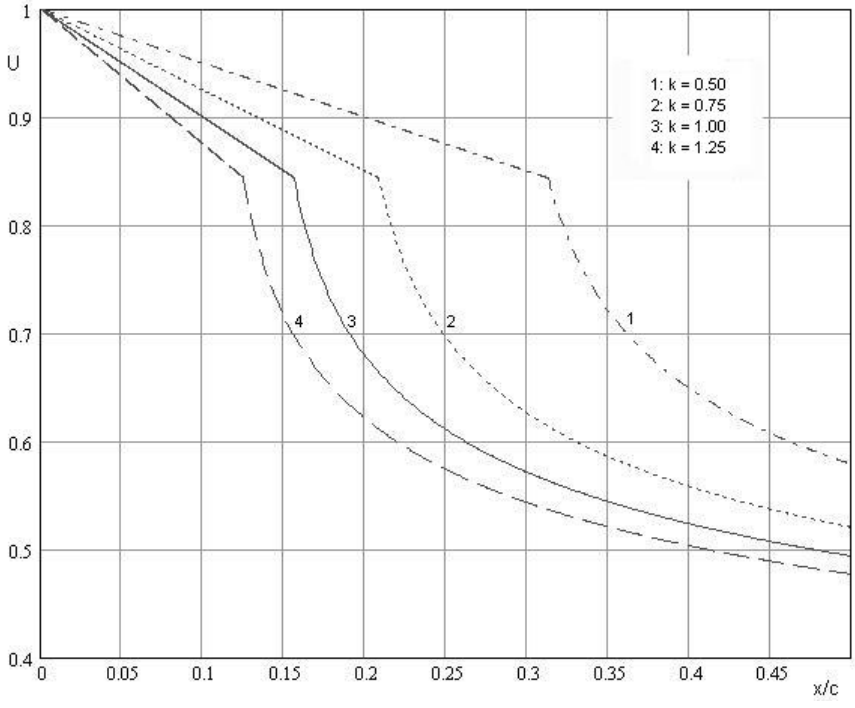

Fig. 3 – Chordwise inviscid velocity distribution for various k.

Figures 3 and 4 illustrate such chordwise inviscid velocity distributions and the corresponding variations of peripheral skin-friction coefficient (C_{fx}) and the boundary-layer shape parameter (H), calculated for various values of k, $\mathrm{Re}_c = 10^6$ and $r/c = \infty$ $(2-D)$. Laminar separation takes place at $C_{fx} = 0$ and a given value of the shape factor, $H = 3.3$, is used as the criterion for turbulent separation/reattachment. Then the skin-friction coefficient is truncated for the above value. The transition point x_t is the point that corresponds to the minimum skin-friction, which here is the point of laminar separation.

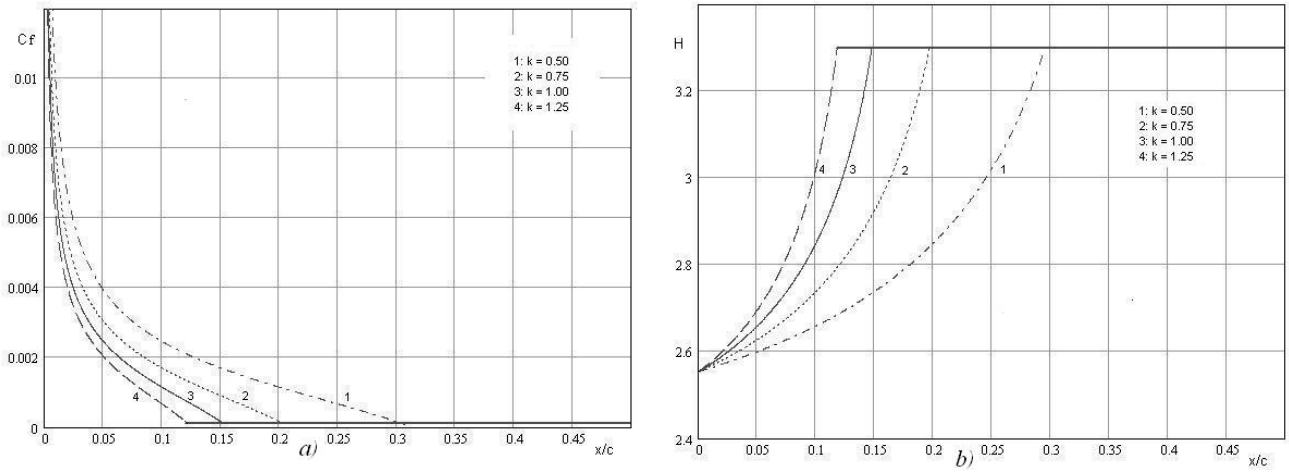

Fig. 4 – Variation of peripheral skin-friction coefficient (*a*), boundary-layer shape parameter (*b*).

The linear adverse velocity gradient assumption is in many cases a satisfactory approximation to the real operating condition and can be used for simulating the velocity distribution in the vicinity of the leading edge of a wind turbine blade subject to leading-edge stall. The extension of the flow after separation with a relaxed flow, that maintains around the leading edge a separating flow state is a satisfactory approximation to the real flow and allows us to use advantageously the boundary-layer model for the analysis of the 3-D separation process. Although different separation patterns may appear on the same body by minor changes in the parameter space of Reynolds number, angle of attack, etc., the essential physical processes which influence the primary flow around blade are not qualitatively affected by these changes.

2.2. Viscous flow

Momentum integral equations. The momentum integral equations for the three-dimensional boundary layer of an incompressible fluid on a rotating blade have been derived by many researcher [1, 9, 10]. The technique presented in this paper is an extension of the method developed by Dumitrescu and Cardos, for a rotating wind turbine in laminar flow [1].

The new features presented now include the incorporation of a three-dimensional entrainment equation and coupling of an inviscid flow near the separation region of the leading edge with the three-dimensional momentum integral equations for boundary layer calculation. The momentum integral equations are obtained by integrating the boundary-layer equations in the normal direction. The resulting two momentum integral equations (one in the mainstream, the other in radial flow direction) are reduced to two first-order partial differential equations using a power law profile for the mainstream velocity, Mager's profile [9] for the cross flow, and a skin-friction relation based on the experimental data of Lakshminarayana and Govindan [10], which is a modification of Ludwieg and Tillmann's [11] skin friction correlation for two-dimensional flows to three-dimensional turbulent boundary layers with pressure gradients, including the effect of rotation. The exponent of the power law for the streamwise velocity component is a function of the local shape parameter (H) which is defined as the ratio of streamwise displacement thickness to streamwise momentum thickness. It thus represents the shape of the streamwise velocity profile.

The coordinate system employed and some of the notations used are shown in Fig. 2, where $x = r\theta$ is the coordinate in the direction of the inviscid streamline at the edge of the boundary layer, r is radial, normal to x, and z is axial, normal to x and the blade surface. The momentum integral equation in x and r directions in the rotating orthogonal coordinate system is given, respectively, by

$$\frac{\partial \delta_{2x}}{\partial x} + \frac{1}{U_e}\frac{\partial U_e}{\partial x}\left(2\delta_{2x} + \delta_{1x}\right) + \frac{\partial \delta_{2xr}}{\partial r} - \frac{\zeta}{U_e}\left(2\delta_{2xr} + \delta_{1r}\right) - 2\frac{\Omega_z}{U_e}\delta_{1r} = \frac{1}{2}C_{fx}, \tag{6}$$

and

$$\begin{aligned}&\frac{\partial\left(\delta_{2xr} + \delta_{1r}\right)}{\partial x} + \frac{2}{U_e}\frac{\partial U_e}{\partial x}\left(\delta_{2xr} + \delta_{1r}\right) + \frac{\partial \delta_{2r}}{\partial r} + \frac{1}{U_e}\frac{\partial U_e}{\partial r}\left(\delta_{2r} + \delta_{1x} + \delta_{2x}\right) - \\ &- \frac{\zeta}{U_e}\left(\delta_{2r} - \delta_{1x} - \delta_{2x}\right) + 2\frac{\Omega_z}{U_e\delta_{1x}} = \frac{1}{2}C_{fr}.\end{aligned} \tag{7}$$

where U_e is the inviscid free stream velocity, $\zeta = \left(\nabla \times \mathbf{V_e}\right)_z = -\frac{1}{r}\frac{\partial}{\partial r}\left(rU_e\right)$, and (C_{fx}, C_{fr}) are the skin friction coefficient components. The usual assumption that the boundary layer is thin compared to the radius of curvature of the blade surface has been made and the arc length *ds* in this coordinate system is given by

$$\mathrm{d}s = \mathrm{d}x^2 + \mathrm{d}z^2 + \mathrm{d}r^2, \tag{8}$$

The various boundary-layer thicknesses are defined as

$$\begin{aligned}&\delta_{2x} = \int_0^\delta \frac{u}{U_e}\left(1 - \frac{u}{U_e}\right)\mathrm{d}z, \quad \delta_{2xr} = \int_0^\delta \frac{v}{U_e}\left(1 - \frac{u}{U_e}\right)\mathrm{d}z, \quad \delta_{2r} = -\int_0^\delta \left(\frac{v}{U_e}\right)^2 \mathrm{d}z, \\ &\delta_{1x} = \int_0^\delta \left(1 - \frac{u}{U_e}\right)\mathrm{d}z, \qquad \delta_{1r} = -\int_0^\delta \frac{v}{U_e}\mathrm{d}z.\end{aligned} \tag{9}$$

A power law type of velocity profile is assumed for the mainstream velocity profile,

$$\frac{u}{U_e} = \left(\frac{z}{\delta}\right)^{(H-1)/2}, \tag{10}$$

where H is the local shape factor.

The assumed cross-flow profile is from [9]:

$$\frac{v}{u} = \varepsilon_w\left(1 - \frac{z}{\delta}\right)^2,$$

where ε_w is the limiting streamline parameter ($\tan\beta_w$).

Equations (6) and (7) can now be written in terms of the parameter δ_{2x}, ε_w, H and C_{fx},

$$\frac{\partial \delta_{2x}}{\partial x} + \left(2 + H\right)\delta_{2x}\frac{1}{U_e}\frac{\partial U_e}{\partial x} + \frac{\partial}{\partial r}\left(L\varepsilon_w\delta_{2x}\right) - \frac{\zeta}{U_e}\left(2L + M\right)\varepsilon_w\delta_{2x} - 2\frac{\Omega_z}{U_e}M\varepsilon_w\delta_{2x} = \frac{1}{2}C_{fx}, \tag{11}$$

$$\begin{aligned}&\frac{\partial}{\partial x}\left[\left(L + M\right)\varepsilon_w\delta_{2x}\right] + \frac{2}{U_e}\frac{\partial U_e}{\partial x}\left(L + M\right)\varepsilon_w\delta_{2x} + \frac{\partial}{\partial r}\left(N\varepsilon_w^2\delta_{2x}\right) + \frac{1}{U_e}\frac{\partial U_e}{\partial r}\left(N\varepsilon_w^2 + H + 1\right)\delta_{2x} - \\ &- \frac{\zeta}{U_e}\left(N\varepsilon_w^2 - H - 1\right)\delta_{2x} + 2\frac{\Omega_z}{U_e}H\delta_{2x} = \frac{1}{2}C_{fx}\varepsilon_w,\end{aligned} \tag{12}$$

where

$$L=\frac{\delta_{2xr}}{\varepsilon_w\delta_{2x}}=\frac{2(7H+15)}{(H+2)(H+3)(H+5)},$$
$$M=\frac{\delta_{1r}}{\varepsilon_w\delta_{2x}}=-\frac{16H}{(H-1)(H+3)(H+5)}, \tag{13}$$
$$N=\frac{\delta_{2r}}{\varepsilon_w^2\delta_{2x}}=-\frac{24}{(H-1)(H+2)(H+3)(H+4)}.$$

The skin-friction relation for flows with pressure gradients and rotation effects is based on the experimental data for a turbulent boundary layer in a rotating channel [9],

$$C_{fx}=0.172\,\mathrm{Re}_{\delta_{2x}}^{-0.268}\,10^{-0.678H}\left(1+B_1\sqrt{\varepsilon_w(x-x_t)/c}\right). \tag{14}$$

This correlation is a modified version of the correlation developed by Ludwieg and Tillmann [10], which includes the effect of rotation. In this relation B_1 is an empiric constant (a value of 0.52 is used), $\mathrm{Re}_{\delta_{2x}}$ is the Reynolds number, based on the streamwise velocity at the edge of the boundary layer and the streamwise momentum thickness δ_{2x}, and x_t is the distance between the leading edge and the transition point along the streamwise direction (the laminar separation point is used).

Closure model-entrainment equation. The pressure gradients cause large changes in velocity profiles and consequently in the shape parameter *H*. The variation of *H* cannot be neglected and an additional equation is required. Out of available auxiliary equations, only the energy integral equation and the entrainment equation have been suitable for the turbulent boundary layers [11]. The former involves more empiricism in calculating the dissipation integral term and assumes the shear stress distribution in the turbulent boundary layer. Since the shear stress variation differs largely from flow to flow, especially those under the influence of rotation and curvature the entrainment equation rather than energy integral equation is used. The entrainment equation is derived from the concept that a turbulent boundary layer grows by a process of entrainment of the inviscid flow at the edge of the boundary layer into the turbulent region, and is obtained from the integration of the continuity equation from the blade surface ($z = 0$) to the edge of the boundary layer ($z = \delta$).

The entrainment equation for the rotor boundary layer in the coordinate system used in this paper can be shown to be

$$\frac{\partial(\delta-\delta_{1x})}{\partial x}+(\delta-\delta_1)\frac{1}{U_e}\frac{\partial U_e}{\partial x}-\frac{\partial\delta_{1r}}{\partial r}+\frac{\zeta}{U_e}\delta_r=C_E, \tag{15}$$

where the entrainment coefficient $C_E\equiv\left(\frac{\partial\delta}{\partial x}-\frac{W_e}{U_e}\right)$ is a function of the factor $H_1=(\delta-\delta_{1x})/\delta_{2x}$. C_E represents the volume flow rate per unit area through the surface $\delta(x,r)$ and is the rate of entrainment of inviscid external flow into the boundary layer.

The entrainment process is a highly complex phenomenon and an empirical correlation for the entrainment function C_E for three-dimensional flow is not yet available. Hence, the entrainment function C_E due to Head [13] for two-dimensional flow is used in the present analysis. The function is given by

$$C_E=0.0306(H_1-3.0)^{-0.653}, \tag{16}$$

Also, the similarity solutions show that H_1 is a function of the streamwise boundary-layer shape parameter *H*. This relationship which results from a best fit to experimental data [14] is

$$H_1 = 2 + 1.5\left(\frac{1.12}{H-1}\right)^{1.093} + 0.5\left(\frac{H-1}{1.12}\right)^{1.093}, \text{ for } H < 4. \tag{17}$$

Then, it is assumed that the variation of the entrainment rate with H_1 follows the same relationship for three-dimensional flows.

Equation (15) is written in a form similar to Eqs. (11) and (12)

$$\frac{\partial}{\partial x}\left(\delta_{2x} H_1\right) + \left(\delta_{2x} H_1\right)\frac{1}{U_e}\frac{\partial U_e}{\partial x} - \frac{\partial}{\partial r}\left(M\varepsilon_w \delta_{2x}\right) + \left(M\varepsilon_w \delta_{2x}\right)\frac{\zeta}{U_e} = C_E\left(H_1\right), \tag{18}$$

Equations (11), (12) and (18) are to be solved for δ_{2x}, ε_w and H (H_1 is related to H, (eq. (17)) with the prescribed boundary conditions. δ_{2x} and ε_w are assumed to be zero at the leading edge and an initial value of 2.55 (laminar flow) is assumed for H.

Numerical procedure. The numerical solution begins from the leading edge of blade by integrating Eqs. (11) and (12) directly, using the laminar boundary layer quantities (9) [1] and an inviscid external linear retarded flow, which after the separation relaxes with the vanishing skin-friction eq. (5). The transition point x_t is chosen to be the laminar separation point and the shape factor H = 3.3 is used to determine the turbulent separation/reattachment point. The initial values for turbulent calculation are determined as a part of the laminar solution for H = 3.5. Method of solution of Eqs. (11), (12) and (18) follows the iterative procedure proposed by Mager [9].

3. RESULTS AND DISCUSSION

Though there are a number of computational aerodynamic analysis (CFD) [14, 15, 16], the exact description of the flow in the vicinity of the rotation center and the physical mechanism which triggers the 3-D and rotational effects are not presently known. Various methods to model the observed effects have been developed [18], [19], but the detailed information of the flow around the rotating airfoil at high angle of attack near the hub is still rather unclear and here a new approach could help.

The results obtained for the leading-edge separation bubbles on a stalled blade suggest a plausible explanation of the rotational augmentation of aerodynamic forces. A key element of this analysis is the determination of the separated area on the blade at leading edge. On the other hand, the whole separation process is a highly complex and inherently unsteady phenomenon and its direct measurement is difficult and confused. In these conditions, the study of 3-D separation process can be advantageously tackled by calling upon a simpler approach based on the solution of the boundary-layer equations according to a particular inverse procedure (eq. (5)). Four cases of severe adverse gradient flow, at leading edge, were analyzed using the described method. The results obtained for the chordwise skin-friction coefficient, the boundary-layer shape parameter, and the limiting streamline angle, at different small values of non-dimensional spanwise distance *r/c* are used to detect and track boundary layer separation and reattachment. In the cases under consideration, the pattern of separation and attachment lines suggests the presence of a conical bubble with high vorticity in the inboard half of the blade and after the bubble breakdown a free-shear layer in the outer part of the blade.

Distributions of the chordwise skin-friction coefficient, C_{fx}, are shown in Fig. 5 at various spanwise distance *r/c* for the value of the velocity gradient parameter k = 1, which corresponds to a severe adverse gradient flow. Points indicated in figure correspond to laminar separation.

The variations of chordwise boundary-layer shape parameter are shown in Fig. 6, which notes the turbulent reattachment points according to constant H criterion. The extent of the separated area, defined as the distance between the separation point x_s and the reattachment point x_r decreases for the decreasing spanwise distance *r/c* and at the limit both points (x_s, x_r) coalesce into a singular point ($C_{fx} = C_{fr} = 0$) with complex structure (a focus-saddle point combination) [2].

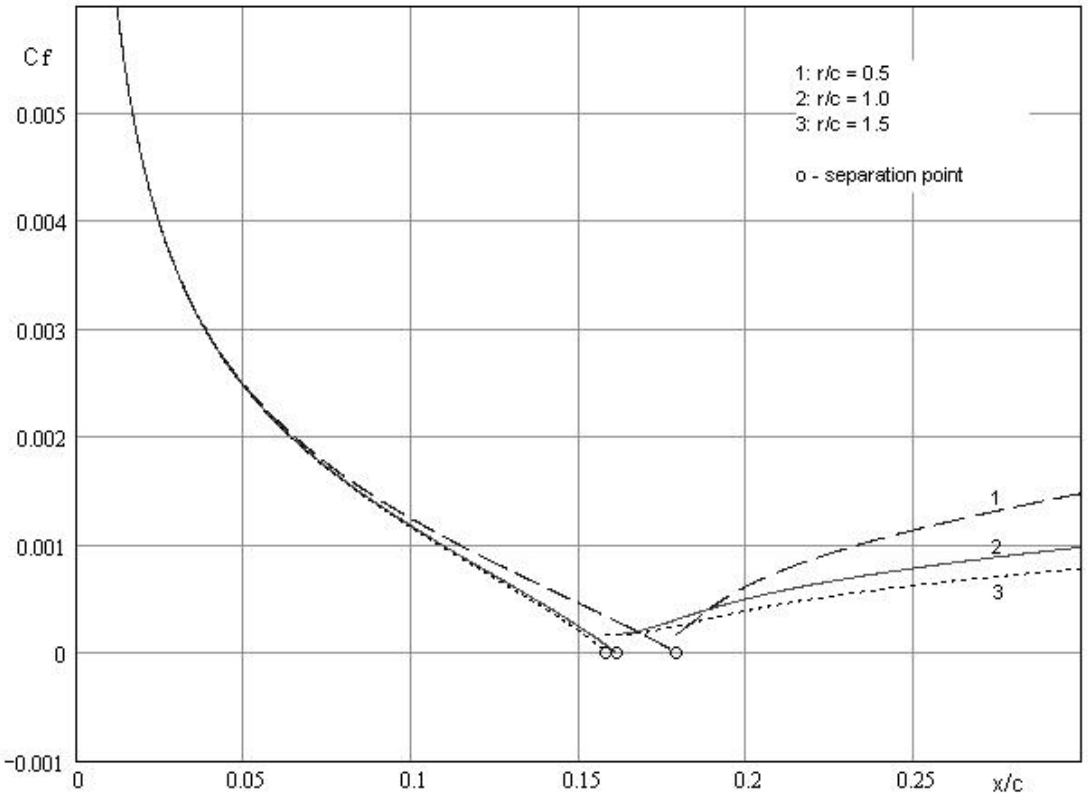

Fig. 5 – Chordwise skin-friction coefficient for various ratios.

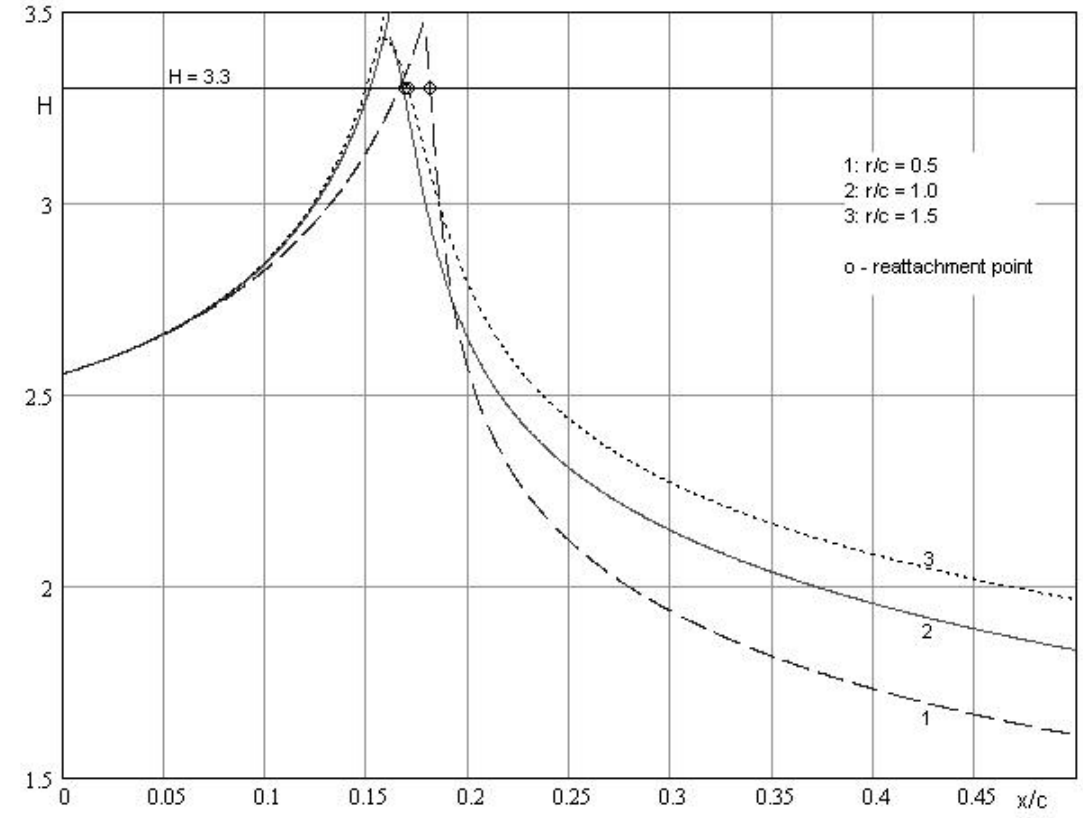

Fig. 6 – Chordwise shape factor for various ratios *r*/*c* and *k*=1.

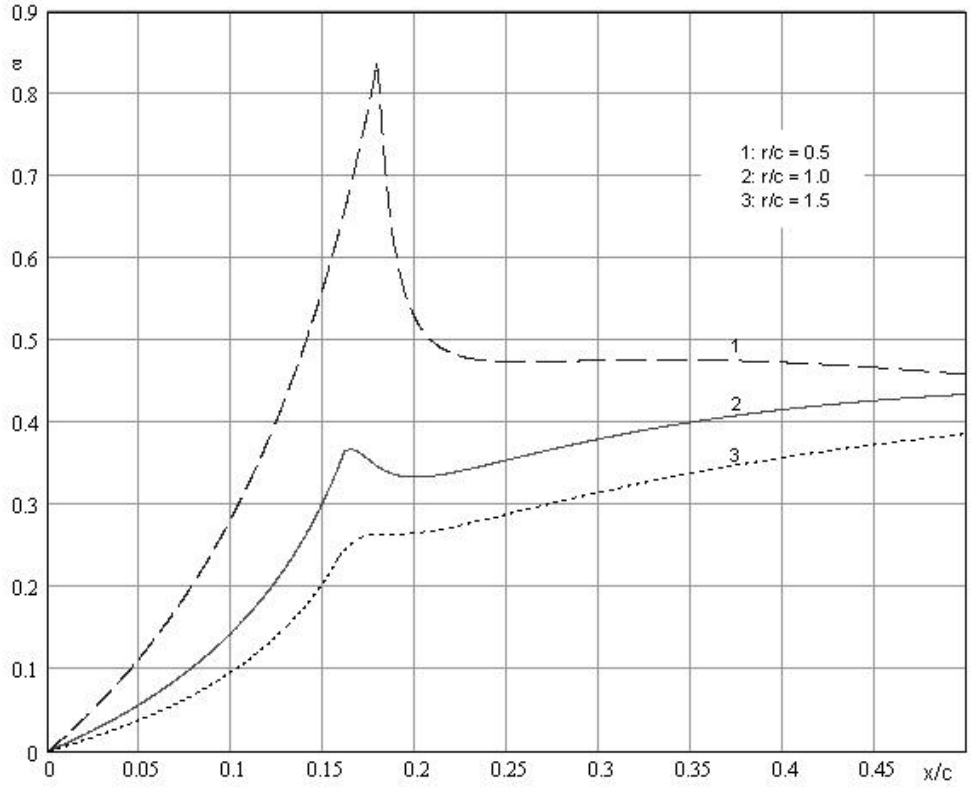

Fig. 7 – Chordwise cross-flow parameter.

In Fig. 7 where variations of cross-flow angle β_w are shown at varying distance from the rotation axis *r/c* an increase of spanwise velocities (and implicitly of Coriolis force) is seen in the separated flow region for decreasing *r/c*.

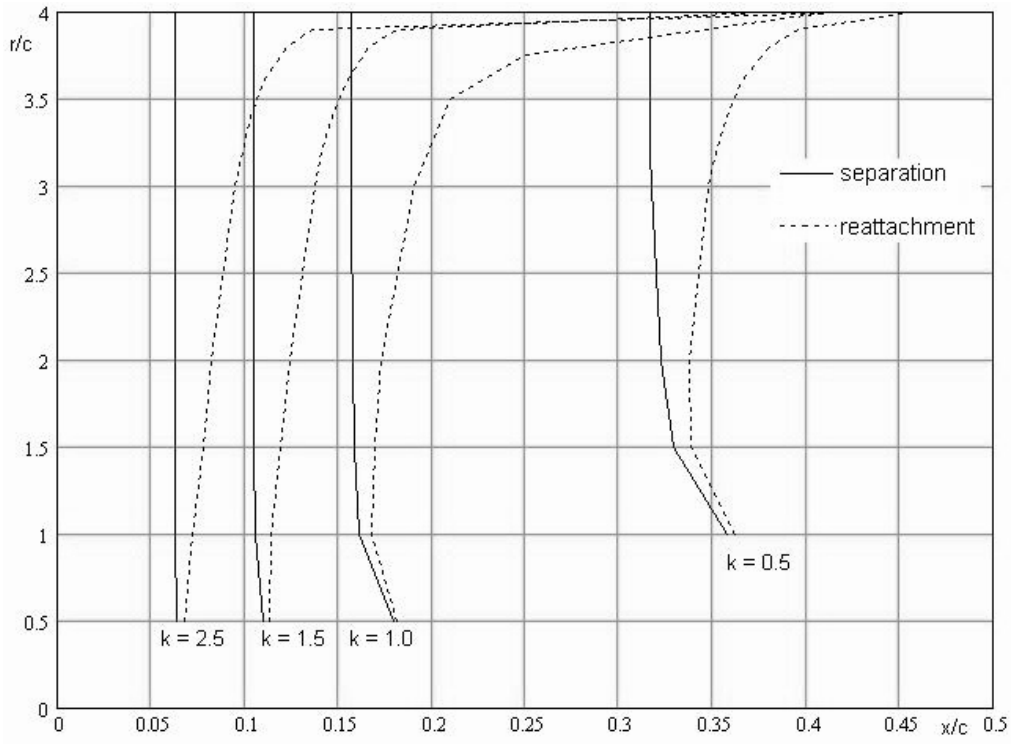

Fig. 8 – Predicted separation/reattachment contours.

Figure 8 shows contours representing rotational leading-edge separation bubbles with high vorticity. The abrupt change in the extent (volume) of the separation bubble observed for all considered cases at approximately r/c = 4 (corresponding to midspan) and near mid-chord could contribute to the bubble breakdown over the suction surface of the blade. The spinning motion like flow in the separation bubble is thought to represent an inboard standing vortex into the streamwise direction which decays immediately when its direction is changed. Indirect evidence of such inboard standing vortex followed by possible vortex bursting is seen in the circulation plot and local values of lift and drag coefficients derived based on the Unsteady Aerodynamic Experiment (UAE) from measurements [20].

At this point in the discussion it is appropriate to interpret the results of this theoretical investigation of three-dimensional blade flow in terms of wall limiting stream lines that may come from a focus-saddle point combination ($C_{fx} = C_{fr} = 0$ with strong vorticity). In the vicinity of the rotation center at the leading-edge the separation leads to a strong vorticity area (theoretical focus point) that starts spiraling off into the flow. Figure 9 gives an impression of the three-dimensional vortex flow structure on the inboard portion of a rotating blade in stall. The separation structure connecting the saddle with the focus contain a line of strong wall streamline convergence on the surface called the separation line (SL) and a line of flow attachment called the reattachment line (RL) near which divergence of wall streamlines occurs. All the streamlines emanating from the saddle point are derived by the Coriolis forces into the singular stream surface enclosing a vortex, called the trapped-vortex bubble (VB). At the middle of blade the vortical bubble breaks down and moves away from the wall, occuring a free-shear layer, i.e. leading-edge stall.

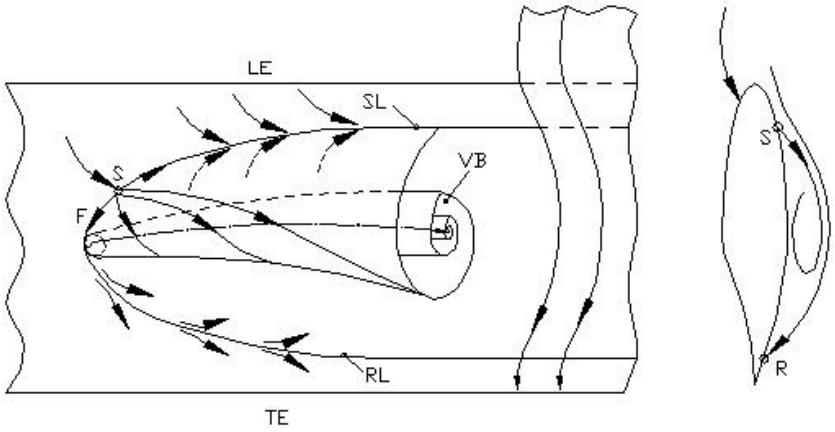

Fig. 9 – Interpretation of the wall limiting streamlines.

The exact theoretical description of the flow around the root of the blade involves doubtless singular points in the flow field that are still rather unclear. Then, probably the most serious deficiency of the study is the inviscid flowfield based on it, which did not have any full separation and wake effects included. Nevertheless, the formulation used here provides a flow whose tangential velocity is governed by conservation of angular momentum, and a chordwise strong adverse velocity gradient at leading-edge that keeps the main features of the real flow.

Physical model of stalled blades. Nowadays, the science of motion rests on three supports which ensure its equilibrium: mathematical modeling, numerical simulation and experiment. However, the very difficult problems require to complete the strict rigor with some heuristic reasoning. The proposed model follows this way to explain the most 3-D and the rotational effects. The flow in the vicinity of leading edge of a blade subject to stall is as sketched to Fig. 10. The central flow around the root of blade ($r/c \approx 1$) converts the axial wind speed into a speedy rotational flow. This is the mechanism that can be attributed to the onset of the three-dimensional and the rotational effects. At the core, the flow acts like a rotating disk in axial flow that pumps the fluid over blades and the large negative pressures, that occur near the leading edge of an airfoil approaching stall, can be considerably reduced on blade. The consequent reduction in the adverse pressure gradient delays/suppresses the separation of the upper surface boundary layer. In this case

the flow near the hub strongly depends on *r/c*, and especially on the rotation parameter $\frac{V_w}{\Omega r}$ [21]. The Reynolds number $\frac{\Omega r^2}{\nu}$ affects mainly the 2D outboard separated flow.

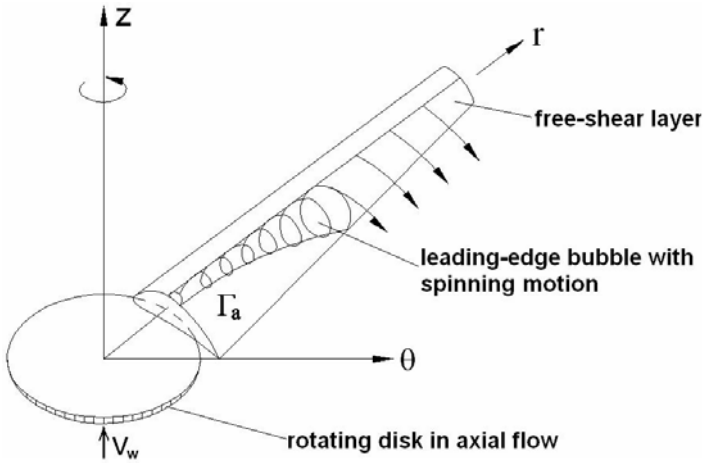

Fig. 10 – Physical model for stalled blades.

Once a small separation bubble is occurred near the leading edge, the Coriolis force sucks mass from the bubble and redirects it to radial direction. The separation bubble is growing and when its volume increases abruptly at about midchord the bubble breaks down and moves away from the wall forming a free-shear layer type separation. The specific mechanism for bubble breakdown that occurs in the midspan region of the blade (*r/c* = 4) is not presently known. It has been postulated, though that there is a physical limitation in the amount of pressure recovery possible in the turbulent shear layer and the Coriolis force, so the bubble bursts when the limit is exceeded and the shear layer fails to reattach. The additional circulation around the inboard blade sections can be explained by the spanwise spinning flow in the leading-edge separation bubble that acts like a standing vortex tending to augment the blade loading and to delay to occurrence of stall. This augmentation of the inboard lift coefficients on rotating stalled blades is consistent with the UAE measurements [20].

If the angles of attack of the blade sections are increased, the bubble moves closer to the leading edge and becomes slightly shorter. Then, before of the bubble breakdown the leading edge bubble has almost no effect on integrated loads, because it is never more than a few percent of the chord length affected by separation.

4. CONCLUSIONS

The momentum integral technique for the wind turbine blade boundary layer has been extended to include the separated and reattaching shear layer in a leading-edge bubble of a wind turbine blade For cases where separated areas exist, a classical boundary layer approach is in principle no more valid (normal pressure gradient, formation of vortices, etc.). However, provided the flow is not widely separated, good description of the viscous effects is obtained, using inviscid flow calculation input. Based on the described boundary layer method, the physical processes which influence the inboard stall-delay phenomenon have been explained, including the onset of the three-dimensional effects and the increase of the lift coefficients. The major conclusions are as follows.

1) The structure of the separated flow on rotating blades in stall is mainly governed by the three most important parameters: *r/c*, $V_w/\Omega r$, Re; *r/c* and $V_W/\Omega r$ have a strong effect on the occurrence of the 3D inboard leading-edge separation bubble (delayed stall) while the 2D outboard separated flow (leading-edge stall) depends especially on Re.

2) Three flow patterns, entirely different can be distinguished: the extreme inboard region ($r/c \le 1$) of unseparated flow like the rotating disk in axial flow, the inboard region ($r/c < 4$) of the three-dimensional flow occupying leading-edge separation bubbles, and the outboard region ($r/c \ge 4$) of two-dimensional separated flow like the free-shear layer.
   Besides, there are two interface flows: one between attached and leading-edge separated flow holding a singular point (focus-saddle point), and another between 3D inboard delayed stall and 2D outboard separated flow (at the mid-span, $r/c \approx 4$), when the bubble breakdown is produced.
3) The conjectured pattern of skin-friction lines near the root of blade ($r/c \le 1.0$), involves a singular point with complex structure, namely a focus-saddle point combination. Physically, this point represents the onset of the leading edge separation bubble which triggers the 3-D and rotational effects
4) It has been shown by a heuristic reasoning that the extreme inboard flow around an airfoil subject to stall angles of attack is fully stabilized against separation due to the rotating disk effect in axial flow.
5) Accurate predictions of stall and post-all airfoil performance at inboard locations must include the induced effects from the spanwise distribution of proper additional circulation.

REFERENCES

1. DUMITRESCU, H., CARDOŞ, V., *Modelling of inboard stall delay due to rotation, The Science of Making Torque from Wind*, Journal of Physics: Conference Series, **75**, 012022, 2007.
2. DUMITRESCU, H., CARDOŞ, V., *Prediction of the three-dimensional separation on a rotating blade*, Int. J. of Applied Mechanics and Engineering, **12**, 4, pp. 941–950, 2007.
3. DUMITRESCU, H., CARDOŞ, V., *Three-dimensional turbulent boundary layer on wind turbine blades*, Annual Meeting of GAMM, Bremen, Germany, April 2008.
4. CARCANGIU, C.E., SORENSEN, J.N., CAMBULI, F., MANDAS, N., *CFD-RANS analysis for the rotational effects on the boundary layer of wind turbine blades, The Science of Making Torque from Wind*, Journal of Physics: Conference Series, **75**, 021031, 2007.
5. CHAVIAROPOULOS, P.K., HANSEN, M.O.L., *Investigating three-dimensional and rotational effects on wind turbine blades by means of quasi-3-D Navier-Stokes solver*, Journal of Fluids Engineering, **122**, pp. 330–336, 2000.
6. DU, Z., SELING, M.S., *The effect of rotation on the boundary layer of a wind turbine blade*, Renewable Energy, **20**, pp. 167–181, 2000.
7. FOGARTY, L.E., SEARS, W.R., *Potential flow around a rotating advancing cylinder blade*, J. Aeronautical Sciences (readers' Forum), **17**, *10*, pp. 599–601, 1950.
8. DRELA, M., *XFOIL- An analysis and design system for Reynolds Number Aerodynamics*, University of Notre Dame, June 1989.
9. MAGER, A., *Generalization of boundary-layer momentum-integral equations to three-dimensional flows including those of rotating systems*, NACA Report 1067, 1951.
10. LAKSHMINARAYANA, B., GOVINDAN, T.R., *Analysis of turbulent boundary layer on cascade and rotor blades of turbomachinery*, AIAA Journal, **19**, *10*, pp. 1333–1341, 1981.
11. LUDWIEG, H., TILLMANN, W., *Investigations of the wall shearing stress in turbulent boundary layers*, Inginieur-Archiv, **17**, pp. 288–299 (NACA TM 1285), 1949.
12 KLINE S, .J., MORKOVIN, M.V., SOVRAN, G., COCKRELL, D.J., eds., *Proceedings of Computation Turbulent Boundary Layers*-AFSOR-IFP, Stanford Conference, Vol. I, Stanford University, 1968.
13. HEAD, M.R., *Entrainment in turbulent boundary layers*, British ARC R&M 3152, Sept. 1958.
14. LOCK, R.C., WILLIAMS, B.R., *Viscous-inviscid interactions in external aerodynamics*, Prgress in Aerospace Sciences, **24**, pp. 51–171, 1984.
15. JOHANSEN, J., SORENSEN, N.N., *Aerofoil characteristics from 3D CFD rotor computations*, Wind Energy, **4**, pp. 283–294, 2004.
16. SCHMITZ, S., CHATTOT, J.J., *Characterization of three-dimensional effects for the rotating and parked NRER Phase VI wind turbine*, Journal of Solar Energy Engineering, **128**, November, pp. 445–454, 2006.
17. VAN ROOIJ, R.P.J.O.M., ARENS, E.A., *Analysis of the experimental and computational flow characteristics with respect to the augmented lift phenomenon caused by blade rotation, The Science of Making Torque from Wind*, Journal of Physics: Conference Series **75**, 012021, 2007.
18. HU, D., HUA, O., DU, Z., *A study on stall-delay for horizontal axis wind turbine blade*, Renewable Energy, **31**, pp. 821–836, 2006.
19. XU, G., SANKAR, L.N., Development *of engineering aerodynamics models using a viscous flow methodology on the NREL phase VI rotor*, Wind Energy, **5**, *2/3*, pp. 171-183, 2002.
20. TANGLER, R., *Insight into wind turbine stall and post-stall aerodynamics*, Wind Energy, **7**, *3*, pp. 247–261, 2004.
21. SCHLICHTING, H., GERSTEN, K., *Boundary layer theory*, Springer Verlag, pp. 328–329, 2000.

Received January 5, 2010